Investigation of Flow Field in Deep Dynamic Stall over an Oscillating NACA 0012 Airfoil

D. Surekha R. S. [1], A. Khandelwal[2,] and R. Rajasekar[3]

[1] *Rajalakshmi Engineering College, Chennai, TamilNadu, India*
[2] *Department of Aerospace Engineering, IIT Kanpur, Kanpur, Uttar Pradesh, India*
[3] *Excel Engineering College, TamilNadu, India*

†*Corresponding Author Email: surekha.aero@gmail.com*

ABSTRACT

This paper presents the investigation on the phenomenon of a deep dynamic stall at the Reynolds number of the order of 10^5 over an oscillating NACA 0012 model. Wind tunnel experiments are conducted to investigate the aerodynamic characteristics of the upstroke and downstroke phase associated with the sinusoidal pitching motion of the airfoil using the technique of surface pressure measurements and Particle Image Velocimetry. The validation of the lift curve slope of upstroke and downstroke with the Prandtl's thin airfoil theory reveals the fact of massive flow separation during the deep dynamic stall regime. Numerical simulations are performed using Reynolds averaged Navier Stokes turbulence models such as RNG K-ε and SST models. The data obtained from these models have been compared with the experimental data to investigate the aerodynamic features of the deep dynamic stall regime. The comparison shows that the URANS with K-ε model is in good agreement with the experimental data within the reasonable regime.

Keywords: Sinusoidal oscillation; Unsteady flow; Pitching airfoil; Numerical simulation.

NOMENCLATURE

a	lift curve slope	u_∞	free stream velocity
c	chord of the airfoil		
C_d	coefficient of drag	$\alpha(t)$	instantaneous angle of attack
C_l	coefficient of lift		
$C_{l,max}$	maximum lift coefficient	ε	turbulence dissipation rate
f	frequency of oscillation	μ	dynamic viscosity
k	reduced Frequency	ρ	density
K	turbulence kinetic energy	ω	angular velocity
Re	Reynolds number	ωt	phase angle

1. INTRODUCTION

The creatures such as birds and marine organisms produce lift and thrust by the flapping mechanism. Being inspired by the flying wing concept, the scientists incorporated the phenomenon of aerodynamics and hydrodynamics of the flapping motion in modern equipment. Recent advances in the performance of micro aerial vehicles have developed the research curiosity in relatively low Reynolds number range of the order 10^5. Analysis of blade element of wind turbine rotors, maneuverable wings, and helicopter rotors has shown that the angle of attack may oscillate under some circumstances. An oscillating airfoil creates load variation which affects the controls of an operating system which was designed based on static loads. Thus, the airfoil when subjected to unsteady motion like oscillating or any other type is dominated by the phenomenon known as the dynamic stall. The factors such as mean angle, the amplitude of oscillation, reduced frequency, Reynolds number, Mach number, the location of pitch axis and the type of pitch motion have a great impact on the unsteady aerodynamics of airfoil oscillating in the pitching motion.

Recently the interest has been provoked in the possible exploitation of the highly energetic nature of this flow in the concept of supermaneuverability of fighter aircraft. Kramer (1932) was one of the first investigators to propose the relation between the coefficient of lift and the angle of attack. He

observed that the coefficient of lift and the angle of attack are directly proportional to each other. The general theory of aerodynamic instability and the mechanism of flutter were first proposed by Theodorson (1949). Carta (1971) proposed a theoretical mechanism for the delay in the dynamic stall. He concluded that the unsteady pressure gradient over the forward portion of the airfoil is less favorable than the steady pressure gradient. According to the study of McCroskey (1981), extensive experiments have been carried out by many researchers to illustrate the complexity of dynamic stall phenomenon but have not led to the understanding needed for the development of satisfactory prediction method. He used the empirical prediction methods to capture the qualitative features of dynamic stall. He also assessed four different regimes such as static stall, onset, light stall, and deep stall regimes experimentally. The reviews by Lawrence (1988); McCroskey (1982) give a good summary of work done in the area of the dynamic stall of an oscillating airfoil. Oshima and Ramapriyan (1992) in their experimental analysis noted that the dynamics of the vortex is associated with the unsteady lift generation and the dynamic stall. Hamdani and Sun (2000) in their work compared the unsteady aerodynamic force obtained by the low and high Reynolds number flow and concluded that the High Reynolds number is responsible for the generation of the new vorticity layer which in turn generates large aerodynamic forces. Deepak and Kamal (2010) experimentally investigated on the effect of flow over the oscillatory motion of airfoil and further determined the quasi-steady and unsteady characteristics in fully and partially developed dynamic stall regimes and tracked the evidence of Laminar Separation Bubble (LSB) and its effect at varied Reynolds number and reduced frequency (κ) for a given oscillating airfoil. Anshul *et al.* (2016) conducted experiments on asymmetric oscillations and stated that the formation, development and the detachment of the Dynamic Stall Vortex (DSV) can be delayed by varying the asymmetric parameter. They had concluded that asymmetry in pitch profoundly affects the hysteresis loop associated with the phase-averaged lift coefficient.

A comprehensive review of different numerical techniques used for analysing dynamic stall phenomenon has been presented by John and Max (1997) which includes deficiencies and scope for improvement of various numerical schemes. Akbari and Price (2003) used a vortex method termed as operator splitting method to solve the two dimensional Navier–Stokes equations. Muti and Pauley (1996) numerically suggested that the unsteady large-scale structure controls the low *Re* separation bubble reattachment with small-scale turbulence play a secondary role. Atluri and Zhu (2000) worked on the meshless method for the moving boundary problems. Yu *et al.* (2010) utilized a high-order spectral difference flow solver and observed the combined effects caused by the reduced frequency and the Strouhal number over the wake vortex structure and thrust coefficient.

Panda and Zaman (1994) studied the lift variation over the cycle of oscillation both computationally and experimentally. They had considered four analytical formulations to estimate the lift from the wake survey. Yongsheng (2011) in his work adopted the technique of overlapping the moving grid for the numerical simulation and investigated the effect of the pitch rate, Reynolds number, and computational domain size over a pitching plate. Surekha and Rajasekar (2015) had computationally analysed the strong dependence of the thrust, lift and propulsive efficiency on the flapping frequency, amplitude and Reynolds number.

Among the available investigations on the oscillating airfoils, most of the studies have performed either purely experimental or only numerical analysis for studying dynamic stall phenomenon. A detailed study using combined experimental and computational can be much useful in shedding light over the physics of unsteady flow separation. Moreover, almost all the research has been concentrated on higher Reynolds number range where flow is entirely turbulent or at very low Reynolds number regime where turbulent effects can safely be ignored. The study of dynamic stall in intermediate Reynolds number range of the order 10^5 where LSB is expected to play a key role has received lesser attention. The current work is aimed to address this research gap, by undertaking experimental along with numerical study of effects of the oscillation in the deep dynamic stall regime at intermediate Reynolds number.

2. EXPERIMENTAL SETUP AND PROCEDURE

Wind tunnel experiments are conducted in a low speed wind tunnel in Low speed Aerodynamics Lab, Department of Aerospace Engineering, IIT Kanpur at the Reynolds number of 1×10^5 and the reduced frequency of 0.1. Reynolds number (Re) is given by the expression,

$$Re = \frac{\rho u_\infty C}{\mu} \tag{1}$$

and the reduced frequency is given by the expression,

$$k = \frac{\omega C}{u_\infty} \tag{2}$$

The test section dimensions are 0.305 m× 1.22 m and free stream turbulence intensity is within 0.25%. The airfoil model of NACA 0012 having a chord length of .16 m and span of .305 m (Fig. 1) is used for experimentation. The description and the nomenclature of the NACA profile are given more elaborately by Ira and Albert (1959).

The airfoil model is designed and fabricated to incorporate the pressure probes at the mid span. The model is designed with 45 pressure ports along the stream wise direction at the mid span crowded near leading edge to capture the phenomenon of surface flow and boundary layer characteristics precisely.

The location of pressure ports has been described by Anshul *et al.* (2016). The fabricated model of NACA 0012 shown in Fig. 2 is made up of acrylic in the middle region and Acrylonitrile butadiene styrene (ABS) in the remaining part.
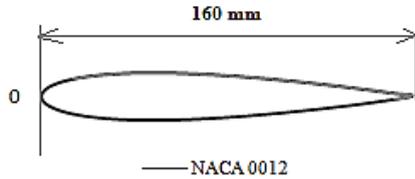
Fig. 1. NACA 0012 of chord 160 mm.

Fig. 2. Fabricated model of the airfoil.

The model is oscillated through the quarter chord point in sinusoidal motion using a scotch-yoke mechanism designed for this purpose. The pressure measurements are done using two piezo-resistive ESP (Electronically Scanned Pressure) scanners, each having 32 pressure ports at a sampling rate of 500 samples/ s for each port. The resolution of pressure measurements from ESP scanners is ± 0.05% of full scale range. Particle image velocimetry (PIV) measurements are carried out using a 2D PIV system from TSI and the associated analysis in Insight 4G software to visualize the chronology of events governing dynamic stall. The data acquisition is done using the NI PXI-6133 14 bit DAQ board from National Instruments Inc. with the help of in-house developed programs in LabVIEW®. A photograph of the instrumented airfoil model mounted in the wind tunnel and is shown in Fig. 3.

Fig. 3. NACA 0012 airfoil model mounted in the wind tunnel with instrumentation for pressure acquisition.
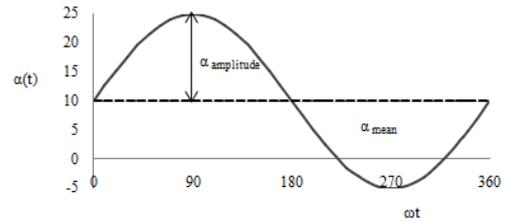
Fig. 4. Angle of Oscillation Vs Phase angle with $\alpha_{mean} = 10°$ and $\alpha_{amplitude} = 15°$.

The sinusoidal motion of the oscillating airfoil is given by,

$$\alpha(t) = \alpha_{mean} + \alpha_{amplitude} \sin(\omega t) \qquad (3)$$

The mean angle of attack is chosen to be 10º because the flow remains attached till 10º for NACA 0012. Since our focus is in the deep dynamic stall regime, the maximum angle of attack is chosen to be more than twice the mean angle of attack; hence the amplitude angle of attack is taken as 15º. Thus, the maximum and minimum angles of attack are 25º and -5º respectively. The geometric blockage at the maximum angle of attack of 25º is about 5.5%.

Figure 4 illustrates the description of the motion of the airfoil. The terms upstroke and downstroke means the situation when the nose of the airfoil moves upwards and downwards respectively. The upstroke motion at a positive angle of attack occurs when the phase angle varies from 0° to 90° and downstroke motion at a positive and negative angle of attack occurs when the phase angle varies from 90° to 180° and 180° to 270° respectively. Finally, the upstroke motion at a negative angle of attack occurs from 270° to 360° of phase angle.

3. NUMERICAL ANALYSIS

The computational fluid dynamics analysis presented in this work are performed using an incompressible Navier Stokes solver. The detailed information of the solver setup can be found in ANSYS (2009). Flow field analysis has been performed using a finite volume discretization of unsteady Reynolds Averaged Navier-Stokes (URANS) equation. Numerical investigation of the behavior of the flow over a low frequency pitching NACA 0012 airfoil at low Reynolds number is performed by the two-dimensional Reynolds Averaged Navier-Stokes (RANS) simulation.

When the local Reynolds exceeds a critical limit, turbulence exists. Even though the Reynolds number taken for investigation is 1×10^5, the deep dynamic stall regime considered for the investigation is viscous dominated. Hence, the turbulence dominated RANS models have been chosen for investigation. RANS models are used to solve the time-averaged Navier Stokes equations. Shear Stress Transport (SST) is selected because it is accurate and robust for low Reynolds number flows whereas Renormalization Group Kinetic energy – dissipation rate (RNG K-ϵ model) is

suitable for the flows with boundary layer separation, vortex shedding and stall. Details of the numerical procedure may be found in Ferziger and Peric (1999).

Grid independence study is carried over in 20000 cells, 22000 cells, 25000 cells, 30000 cells and by referring to McAlister *et al.* (1978) it is found that the static results obtained in this paper give good agreement with the 25000 cells. The solution converges and is consistent beyond 25000 cells. Thus the grid shown in Fig. 5 is chosen as the best-optimized grid.
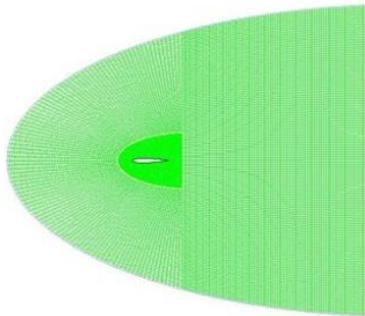
Fig. 5. Optimized grid with 25000 cells.

The laminar kinetic energy and turbulent kinetic energy on the airfoil are zero; hence the no-slip condition is imposed on the airfoil. The laminar kinetic energy in the free stream is zero because it is considered to be far away from the boundary layer. In order to perform the unsteady flow condition, the dynamic finite volume mesh is enabled. The domain consists of the movable interior region with the airfoil and the static exterior region. In order to simulate the sinusoidal motion of the airfoil, the movable interior region is set as a deforming body with the rigid body airfoil. As the interior region moves, the airfoil moves with it. The interpolation points between the grids are recalculated and the whole mesh is regenerated by the phenomenon of dynamic mesh. The sinusoidal oscillation is made possible by compiling a user-defined function. The domain optimization study was carried over for various domain sizes and finally, the domain shown in Fig. 5 is considered as the optimized domain based on its convergence and its agreement with the results given by McAlister *et al.* (1978).

4. RESULTS AND DISCUSSION

The events associated with the dynamic stall have been studied by both the experimental and computational analysis. The comparison has been made in the results so as to comment on the efficacy of the chosen turbulent model.

4.1 Dynamic Stall Process

The mean angle of attack and the amplitude angle of attack chosen for our investigation are 10° and 15° respectively. Hence, the maximum angle of attack is 25° which is far above the static stall angle. The maximum angle of attack is the primary

parameter that determines the degree of separation of the flow. A large increase in maximum angle of attack well beyond the static stall angle leads to the deep dynamic stall regime, which results in the large viscous zone over the entire upper surface of the airfoil during the upstroke motion of the cycle. The deep dynamic stall is characterized by the process of the formation and shedding of a huge Leading Edge Vortex (LEV) that carries a low-pressure wave sweeping over the aerofoil along the suction surface of the airfoil as elaborated by McCroskey (1981).

(a) α(t) = 15º

(b) α(t) = 20.5º

(c) α(t) = 23.5º

(d) α(t) = 25º
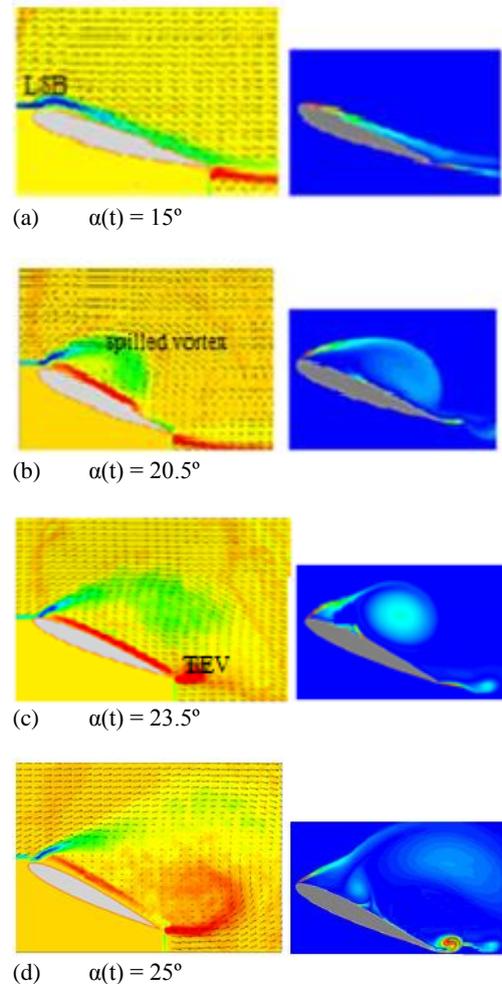
Fig. 6. Vorticity field of PIV and computational data of the SST model at different instantaneous angle of attack.

This phenomenon produces the values of C_l and C_d far in excess of their static values and a large amount of hysteresis occur during the rest of the cycle. As the airfoil pitches well beyond the static stall angle, the unsteady separation process leads to the formation of the LEV. The LEV plays an important role in the dynamic stall process, whereas the trailing edge flow plays an indirect, rather the least role in the dynamic stall process. Figure 6 shows the formation and movement of the vortices at different angles of attack with a comparison between phase-averaged experimental and computational results. The flow field in the

computational results of the SST turbulence model agrees well with the experimental result.

For the angle of oscillation below the static stall angle of 11.5°, the flow remains attached. When α reaches 15°, the flow reversal takes place in the boundary layer, however, the boundary layer still remains thin and attached due to unsteady effects. The formation of LSB at α= 15° can be seen from Fig. 6(a). The LSB continues to increase in size and grow into LEV. Following the flow separation at the leading edge, the formation of spilled vortices at the angle of attack of 20.5° is clearly shown in Fig. 6(b). The initial breakdown appears with the separation of the LEV. The size of LEV is observed to grow with the increase in the angle of oscillation. Further increase in angle of oscillation to 23.5° leads to the convection of the vortex over the chord. This phenomenon where the flow remains attached much beyond the static stall angle during the formation and convection of vortex leads to augmentation in the lift. Figure 6(c) shows the vortex convecting over the airfoil. This phenomenon where the flow remains attached much beyond the static stall angle during the formation and convection of vortex leads to augmentation in the lift is a marked characteristic of deep dynamic stall. The maximum lift coefficient attained experimentally during upstroke by pitching the airfoil is 1.6, which is far in excess of the maximum static lift coefficient. Moreover, the presence of DSV near trailing edge induces a formation of trailing edge vortex, as depicted in Fig. 6(c). Further increasing the angle of attack beyond 23.5° leads to lift stall. At this stage, the vortex reaches the trailing edge and the flow progresses to a state of complete separation. The flow becomes completely separated over the upper surface of the airfoil at the maximum angle of attack of 25° (Fig. 6(d)) and continues to remain separated over a substantial time during the downstroke phase of oscillation. This flow separation tends the curve to follow a different pattern during the downstroke which results in the large hysteresis loop even though the oscillation is simple harmonic. Flow reattachment during downstroke phase starts below the static stall angle.

4.2 Aerodynamic Forces

Figure 7 shows the comparison of the lift coefficient obtained from the two-dimensional simulations using RNG K-ϵ and SST models with the experimental data. In general, the dynamic stall obtained is delayed well beyond the static stall angle and a large amount of hysteresis loops are well predicted. The dynamically pitching airfoil gives higher lift than the static airfoil held at a constant angle of attack. It can be seen that for upstroke from -5° to 22°, RNG K-ϵ and SST models follow the same trend. Beyond 22°, for RNG K-ϵ at 23.5°, $C_{l, max}$ of 1.84 was obtained, whereas $C_{l, max}$ of 2.35 was obtained at 24.5° for the SST model. The two models present a satisfactory agreement with the experimental data till 21.5°, where $C_{l, max}$ is obtained. The peak value of the coefficient of lift obtained by RNG K-ϵ is close to the experiments. However at large angle of incidence in the upstroke (21.5° < α <23.5°), the computed curve of SST

model diverge and the coefficient of lift overshoots, whereas the computed curve of RNG K-ϵ follows the same pattern. Beyond 23.5°, SST model presents a too sharp drop off of C_l shortly after the lift stall occurs. This drop in lift coefficient at the critical angle of oscillation is due to complete separation of the boundary layer from the upper surface of the airfoil leading to a full stall condition. During the upstroke, the lift coefficient linearly increases with the angle of attack until the DSV sheds. This is characterized by the shedding off large vortices from the leading edge. Table 1 gives the value of the maximum coefficient of lift and its corresponding angle of attack.

During the downstroke phase (25° < α < -5°), the computed curve of RNG K-ϵ turned predicts earlier reattachment and thus is different from the curves of SST and experiments. On the other hand, SST model leads to rise in lift again for a period during downstroke because of formation of secondary LEV, not present in experimental results. Thus, the lift curves of both models do not agree very well with the experimental results. Hence in general, the prediction RANS (unsteady) with K-ε model is fairly good with the experimental data.

In addition to the above, it is also observed that the upstroke motion satisfies the important results of Prandtl's thin airfoil theory. According to the theory, the lift curve slope (a) shown in Eq. (4), should be 0.11/degree.

$$Lift\ slope, \qquad a = \frac{dC_l}{d\alpha} \qquad (4)$$

Table 1 $C_{l, max}$ and its corresponding α for various cases at κ=0.1

Description		α	$C_{l, max}$
Static stall	Experimental	11°	0.8
	Computational	12.5°	0.85
Dynamic Stall	Experimental	21.5°	1.6
	SST	24.5°	2.35
	RNG K-ϵ	23.5°	1.84

There are significant differences in the lift curve slope of upstroke and downstroke. These are examined in Table 2. It compares the lift curve slope of the upstroke and downstroke phase with the Prandtl's thin airfoil theory. The lift curve slopes at the reduced frequency of 0.1 for the upstroke phase in all the three cases satisfies the approximation of thin airfoil theory. This gives additional information that the procedures followed to obtain these results are proper. In contrast, the lift curve slope of the downstroke phase does not satisfy the theory. There is a noteworthy lag in the slope during the downstroke. The offset of the downstroke is considerably large. This signifies that the flow is highly disturbed during the downstroke

and hence becomes more diffusive, which results in the lag of the lift curve slope.
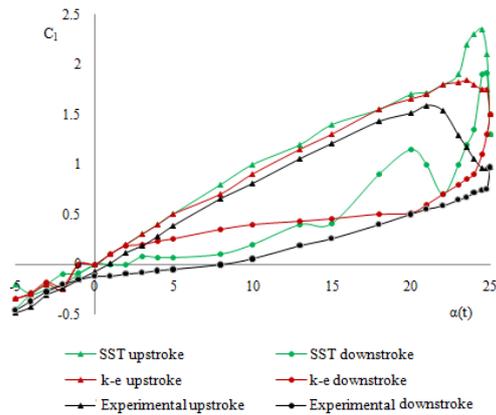
Fig. 7. Comparison of the determined PIV and numerical data of C_l versus α (t) for k=0.1, Re=1 X 10^5.

Table 2 Lift curve slope at the k=0.1

Description	Upstroke	Downstroke	
	a (/°)	a (/°)	offset
Experimental	0.06	0.03	0.08
SST	0.08	0.01	0.03
RNG K-ϵ	0.079	0.03	0.038

Comparing the C_d curves, it can be observed that the value of C_d rises earlier for experimental results due to earlier dynamic stall, whereas the URANS models assuming fully turbulent flow everywhere predict dynamic stall at a later angle. Even though RNG K-ϵ model accounts for low Reynolds number effects, the C_d - α curve obtained during upstroke and downstroke is far dissimilar from the experimental data, whereas SST model shows a better agreement with the experimental data during downstroke motion. This is because the SST model gives accurate predictions on flow separation under adverse pressure gradients since it includes the transport effects into the formation of eddy viscosity. In addition to RNG K-ϵ, SST model also shows a great variation with the experimental data for C_d curve. The hysteresis loop obtained by the experimentation is quite large, implying significant hysteresis between upstroke and downstroke motions. Comparatively, the hysteresis loop is much smaller in both SST and RNG K-ϵ models. Unlike the C_l - α curve, the upstroke and the downstroke motion follows the same path in C_d - α curve obtained by the SST model. A part of the discrepancy between experimental and computational results may also arise from the fact that experimental results consider only the pressure drag term neglecting the contribution from viscous terms. The curve also reveals the fact that the coefficient of drag has nearly the same value of 0.5 for all the three curves at the highest angle of attack during upstroke motion.

As stated by Von Karman and Burgers (1934),

Garrick (1937), it is observed from Fig. 8, that the coefficient of drag obtained in all the three cases always remain positive which confirms that the thrust is never produced by pitching the airfoil at a reduced frequency of 0.1. In the case of the SST turbulence model, the maximum coefficient of lift of 2.3 is obtained at an angle of attack of 24° and the corresponding co-efficient of drag is 1.2, whereas, in case of RNG K-ϵ model at 23.5°, the maximum co-efficient of lift of 1.84 is obtained and the maximum co-efficient of drag of 0.5 is obtained at 25° of angle of attack.
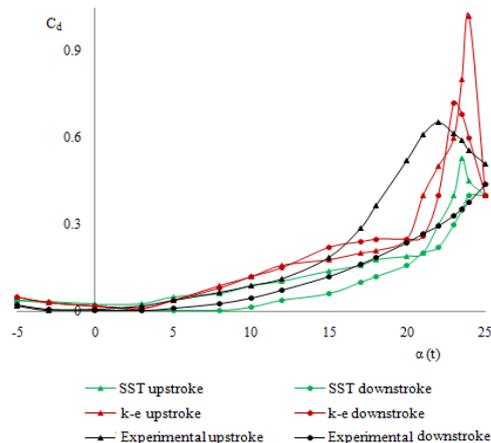
Fig. 8. Comparison of the determined PIV and numerical data of C_d versus α (t) for k=0.1, Re=1 X 10^5.

5. CONCLUSIONS

Experimental investigation of the two-dimensional low Reynolds number flow around an oscillating airfoil has been performed to study the effect of the sinusoidal motion of the airfoil. Two turbulence models SST and RNG K-ϵ models have been employed to simulate two-dimensional fluid flow around the NACA 0012 airfoil, executing a sinusoidal motion in the deep stall regime. In general, both the models employed show reasonable agreement with the experimental analysis during the upstroke except at very high angle of attack where the flow is completely detached and three-dimensional effects are known to be quite significant. The characteristics of the deep dynamic stall have been well captured by PIV and SST turbulence models. The lift curve slope of the upstroke obeys Prandtl's lifting line theory whereas the downstroke fails due to the massive flow separation on the upper surface. In order to obtain a very detailed understanding of the dynamic stall phenomenon, more advanced methods need to be examined. However, from this study, we can conclude that RANS models are capable of capturing a significant part of the flow dynamics of the dynamic stall.

REFERENCES

Akbari, M. H. and S. J. Price (2003). Simulation of

dynamic stall for a NACA 0012 airfoil using a vortex method. *Journal of Fluids and Structures* 17, 855-874.

Anshul, K., K. Poddar and D. Das (2016). Investigations into Asymmetric Oscillations of a Symmetric Airfoil. *Fluid Mechanics and Fluid Power – Contemporary Research*. Lecture Notes in Mechanical Engineering. Springer.

ANSYS (2009). ANSYS Fluent 12.0 Theory guide, ANSYS Inc., USA.

Atluri, S. N. and T. Zhu (2000). New concepts in meshless methods. *International Journal of Numerical Methods in Engineering* 47 (1-3), 537-556.

Carta, F. O. (1971). Effect of Unsteady Pressure Gradient Reduction on dynamic Stall Delay. *Journal of Aircraft* 8 (10), 839-840.

Deepak, K., M. Sharma and K. Poddar (2010). Investigations on quasi-steady characteristics for an airfoil oscillating at low reduced frequency. *International Journal of Aerospace Engineering* 2010,1-11.

Ferziger, J. H. and M. Peric (1999). *Computational method for fluid dynamics*. Springer, New York

Garrick, I. E. (1937). *Propulsion of a flapping and oscillating airfoil*, NACA Technical Report No. 567.

Hamdani, H. and M. Sun (2000). Aerodynamic forces and flow structures of an airfoil in some unsteady motions at small Reynolds number. *Acta Mechanica* 145, 173-187

Ira. H. Abbott and Albert. E. Doenhoff (1959). *Theory of wing sections*, Dover Publications, Inc. Newyork.

John, A. E. and Max .F .Platzer, (1997). Computational prediction of airfoil dynamic stall. *Progress in Aerospace Sciences* 33, 759-846

Kramer, M. (1932). *Increase in the maximum lift of an airplane wing due to a sudden increase in its effective angle of attack resulting from gust*. NASA Technical Memorandum 678.

Lawrence, W. C. (1988). Progress in analysis and prediction of dynamic stall. *Journal of Aircraft* 25 (1), 6-17.

McAlister, K. W., L. W. Carr and W. J. McCroskey (1978). *Dynamic Stall Experiments on the NACA 0012 Airfoil*. NASA TP 1100.

McCroskey, W. J. (1981). *The phenomenon of Dynamic stall*, NASA Technical Memorandum 81264.

McCroskey, W. J. (1982). Unsteady airfoils. *Annual Review of Fluid Mechanics* 14, 285-311.

Muti Lin, J. C. and L. L. Pauley (1996). Low Reynolds number separation on an airfoil. *American Institute of Aeronautics and Astronautics* 34 (8), 1570-1577.

Oshima, H. and B. R. Ramapriyan (1992). Measurements of the velocity and vorticity fields around a pitching airfoil. *American Institute of Aeronautics and Astronautics* 92, 251-259.

Panda, J. and K. B. M. Q. Zaman (1994). Experimental Investigation of the Flow Field of an Oscillating Airfoil and Estimation of Lift from Wake Surveys. *Journal of Fluid Mechanics* 265, 65-95.

Surekha Rathi Samundi, D. and R. Rajasekar (2015). Aerodynamic response for an oscillating airfoil in steady flow. *International Journal of Applied Engineering Research* 10 (62), 99-103.

Theodorsen, T. (1949). *General Theory of Aerodynamic Instability and then Mechanism of Flutter*, NACA Report No. 496.

Von Karman, T. and J. M. Burgers (1934). *General aerodynamic theory - perfect Fluids*, Aerodynamic Theory 2, W. F. Durand (Ed.), Julius Springer: Berlin, 308.

Yongsheng, L. (2011). Parametric study of a pitching flat plate at low Reynolds number. *Computer Modeling in Engineering and Sciences* 72 (1) , 1-16.

Yu, M. L., L. Hu and Z. J. Wang (2010). *A numerical study of vortex-dominated flow around an oscillating airfoil with high order spectral difference method*, 48th AIAA Aerospace Sciences Meeting. Florida.